Nano Research 2015, 8(11): 3694–3703
DOI 10.1007/s12274-015-0869-9
Research Article
ISSN 1998-0124
CN 11-5974/O4

Large-area growth of ultra-high-density single-walled carbon nanotube arrays on sapphire surface

Lixing Kang[1,2,3], Yue Hu[2], Hua Zhong[4], Jia Si[4], Shuchen Zhang[2], Qiuchen Zhao[2], Jingjing Lin[2], Qingwen Li[1] (✉), Zhiyong Zhang[4], Lianmao Peng[4], and Jin Zhang[2] (✉)

[1] *Division of Advanced Nanomaterials, Suzhou Institute of Nanotech and Nanobionics, Chinese Academy of Sciences, Suzhou 215123, China*
[2] *Center for Nanochemistry, Beijing Science and Engineering Technology Research Center for Low Dimensional Carbon Materials, College of Chemistry and Molecular Engineering, Peking University, Beijing 100871, China*
[3] *University of Chinese Academy of Sciences, Beijing 100049, China*
[4] *Key Laboratory for the Physics and Chemistry of Nanodevices, Department of Electronics, Peking University, Beijing 100871, China*

Received: 13 June 2015
Revised: 10 July 2015
Accepted: 17 July 2015

KEYWORDS
single-walled carbon nanotube arrays,
ultra-high density,
large area,
cooperating catalysts

ABSTRACT

A scalable approach to obtaining high-density, large-area single-walled carbon nanotube (SWNT) arrays is essential for realizing the full potential of SWNTs in practical electronic devices; this is still a great challenge. Here, we report an improved synthetic method for large-area growth of ultra-high-density SWNT arrays on sapphire surfaces by combining Trojan catalysts (released from the substrate, to assure ultra-high density) with Mo nanoparticles (loaded on the surface, to stabilize the released Trojan catalysts) as cooperating catalysts. Dense and perfectly aligned SWNTs covered the entire substrate and the local density was as high as 160 tubes/μm. Field-effect transistors (FETs) built on such arrays gave an output current density of −488 μA/μm at the drain-source voltage (V_{ds}) = the gate-source voltage (V_{gs}) = –2 V, corresponding to an on-conductance per width of 244 μS/μm. These results confirm the wide range of potential applications of Trojan-Mo catalysts in the structure-controlled growth of SWNTs.

1 Introduction

Horizontally aligned single-walled carbon nanotube (SWNT) arrays on flat substrates are suitable candidates for the fabrication of integrated circuits, because of their superior electrical properties [1–3]. However, one of the key challenges in achieving sufficient current output and large-scale device integration is placing the SWNTs at a very tight (5–10 nm) pitch with good alignment, to enable density scaling and source/drain contact scaling; the SWNT array density must be 100–200 tubes/μm [4, 5]. Two techniques have been developed to achieve this goal. One involves post-treatment approaches such as multiple transfer [6, 7] and solution-based SWNT placement methods [8–12]. These approaches significantly increase the SWNT density, which can reach 500 tubes/μm [8], and there is no limit to the assembly area, but the

Address correspondence to Jin Zhang, jinzhang@pku.edu.cn; Qingwen Li, qwli2007@sinano.ac.cn

tubes in post-treatment processes are always defective and poorly orientated, which severely degrades the performances of SWNT devices. The second technique, i.e., direct chemical vapor deposition (CVD) growth, produces high-quality, perfectly aligned SWNTs on substrates [13–15].

In recent years, rapid progress has been made in CVD methods for the growth of dense, perfectly aligned SWNT arrays on quartz or sapphire substrates [16–18]. In a CVD system, the density and area of a SWNT array largely depend on the activity and aggregation of catalysts [19, 20]. Methods for maintaining uniform distribution of catalysts over large areas and preventing catalyst aggregation and poisoning during SWNT growth are always being developed [21–23]. Many groups have proposed various solutions such as using monometallic catalysts (i.e., Fe, Co, and Cu) through sequentially patterning catalysts [23], periodic growth [24], and multiple-cycle growth [25]. Large-area, high-quality, aligned SWNTs have been successfully obtained on quartz substrates. However, the density only reached 10–60 tubes/μm, which is far short of the requirement for superior device performances. In these reported methods, the catalysts were all simultaneously exposed to the growth atmosphere during the initial SWNT growth process; this caused lateral diffusion and sintering. Most catalysts were therefore deactivated before they could catalyze the growth of SWNTs. These drawbacks were the main reasons for the low density. Recently, our group developed a new method for preparing catalysts called Trojan catalysts. This method is effective for growing SWNT arrays with density as high as 130 tubes/μm on sapphire surfaces [26]. Briefly, Fe catalysts are dissolved in the substrate and stored, and then can be released gradually during SWNT growth. Note that all the Trojan catalysts mentioned in this paper consist of Fe nanoparticles dissolved in a sapphire substrate, unless otherwise specified. This gradual-release mode decreased interactions among the Trojan catalysts and ultra-high-density SWNT arrays were eventually obtained. The dissolve-and-release process prevented the aggregation of some of the Trojan catalysts and improved the catalytic efficiency to some extent, but some of the released Trojan catalysts still tended to migrate and merge, which restricted the area of high-density SWNT arrays. The SWNT array widths were generally in the range several hundreds of microns, which severely limited their use in large-scale device integration. Recently, we found that the surface structure of the substrate greatly influenced the growth of SWNTs. Terrace-step-kink sites were formed on the substrate surface after annealing. These terrace-step-kink sites were along with unsaturated bonds or dangling bonds, providing more adsorption sites for the released Trojan catalysts. The released Trojan catalysts were pinned to these sites, enabling formation of high-density SWNT arrays. The inhibition of catalyst aggregation on flat substrates during CVD processes is therefore a key issue in obtaining large-area SWNT arrays with ultra-high density.

It is well known that combined Fe–Mo catalysts can promote SWNT growth, because Mo catalysts can stabilize active Fe nanoparticles in CVD systems [27–29]. In this study, we developed a method that combines Trojan catalysts (which are released from the substrate, to ensure ultra-high density) with Mo nanoparticles (which are loaded on the surface, to stabilize the released Trojan catalysts) as cooperating catalysts (we named the synergistic catalysts Trojan-Mo catalysts) for growth of large-area, ultra-high-density SWNT arrays. Figure 1 schematically illustrates the procedure for this method. First, the Trojan catalysts were prepared using a previously reported method [26]. The Fe catalysts were annealed (at 1,100 °C in air for 8 h) to dissolve them into an *a*-plane sapphire substrate. The precursors of the Mo catalysts were then dispersed on the substrate. The sapphire substrates containing the Trojan-Mo catalysts were then placed in a CVD system for the growth of SWNT arrays (the details are given in the experimental section). When

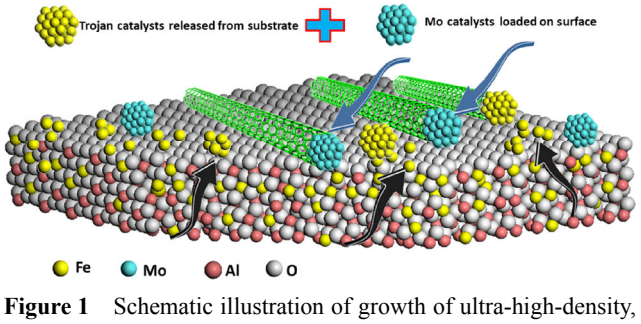

Figure 1 Schematic illustration of growth of ultra-high-density, horizontally aligned, single-walled carbon nanotube arrays using Trojan-Mo catalysts.

Fe was released gradually from the substrate and started to form Fe nanoparticles, some of the Mo nanoparticles formed nuclei for SWNT growth. Migration and agglomeration of the released Fe nanoparticles were effectively suppressed by the Mo catalyst nanoparticles, and the nanotubes grew from them. The introduction of Mo catalysts on the surface pins the released Trojan catalyst and creates more opportunities for SWNT nucleation; this aids expansion of the SWNT array growth areas while retaining ultra-high density.

2 Results and discussion

The use of Trojan-Mo catalysts enabled an entire sapphire wafer (15 mm × 30 mm, Fig. 2(a)) to be covered with ultra-high-density SWNT arrays, as shown by scanning electron microscopy (SEM; Figs. 2(b) and 2(c)); this was confirmed using Raman spectroscopy [30]. Figure 2(d) shows a typical Raman spectrum at 514.5 nm excitation. Clear radial breathing mode peaks in the low-frequency region and a barely noticeable defect-induced D band at ~1,350 cm^{-1} indicate that high-quality SWNTs were synthesized on the sapphire substrate. SEM and atomic force microscopy (AFM) are the two most commonly used techniques for characterizing horizontal SWNT arrays [31–33]. Because of electron-beam-induced charge accumulation within the insulating sapphire substrate, the sapphire surface around the SWNTs was imaged instead of the SWNTs themselves. The SWNTs therefore appeared thicker in the SEM images [34]. The width of an individual nanotube after gold sputtering was about 10 nm for 1 keV electrons in the SEM image. For ultra-high-

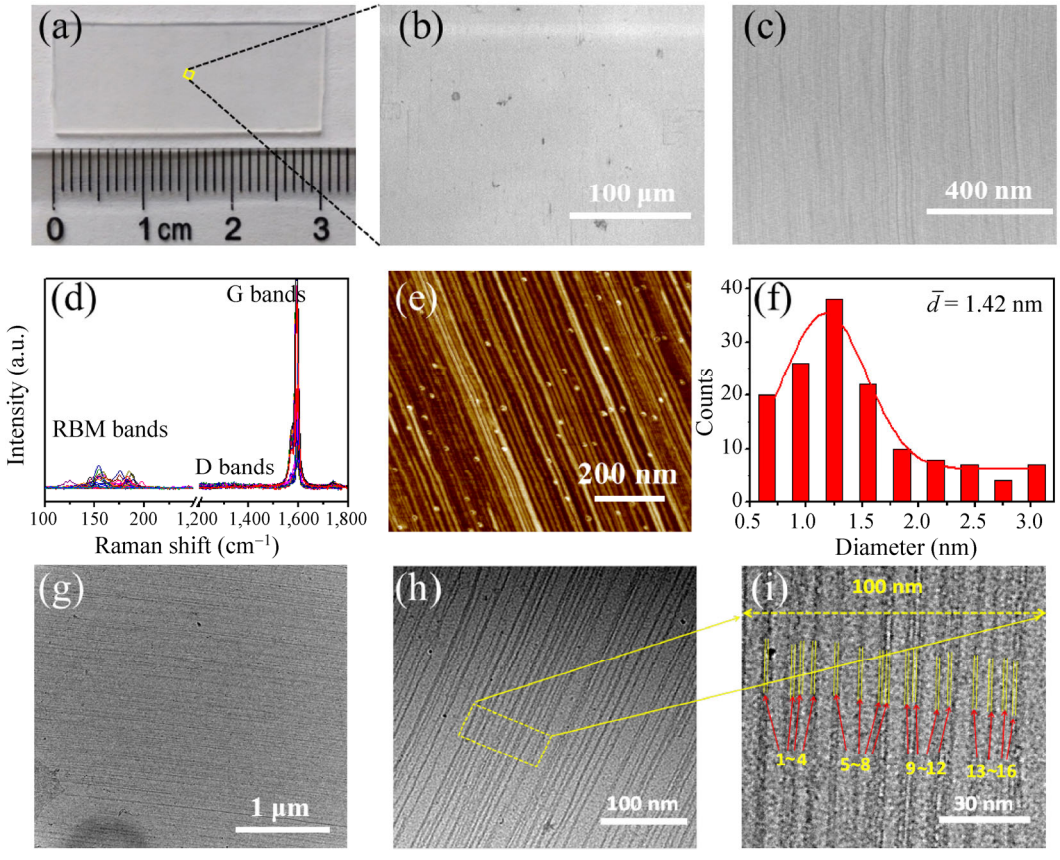

Figure 2 Photograph (a) and SEM images ((b) and (c)) of SWNT arrays obtained using Trojan-Mo catalysts, with super high density and uniform dispersion on the wafer. (d) Raman spectrum of as-grown SWNTs at 514.5 nm excitation. (e) Typical AFM image of as-grown SWNT arrays. (f) Corresponding diameter distribution of SWNTs. Red solid line is Gaussian fitting peak. (g)–(i) HRTEM images of ultra-high-density SWNT arrays transferred onto ultra-thin carbon membrane supported on Cu grid at low and high magnifications. HRTEM image (i), at higher magnification, confirms that the density of SWNT arrays is as high as 160 SWNTs/μm (each of 16 SWNTs in100 nm length area has been marked in (i)).

density SWNT arrays (ideal value >100 tubes/μm) on sapphire, the SWNT images overlap and form a continuous film under high magnification, as shown in Fig. 2(c). The density of the SWNT arrays was therefore too high to be accurately measured using SEM. However, SEM is still a fast and convenient method for the determination of array area and uniformity on the micron scale. Similar SEM images were obtained over the whole substrate (Fig. S1 in the Electronic Supplementary Material (ESM)), confirming uniform density dispersion with large-area coverage. The distance between two SWNTs in the samples was smaller than the AFM tip (radius of curvature ~10 nm), which led to a large convolution effect and loss of lateral resolution [35]. The SWNT arrays in AFM images at different magnifications (Figs. 2(e) and Fig. S2 in the ESM) both approached a full monolayer. AFM was therefore affected by the decline in the lateral resolution power and tended to underestimate the array density. The AFM height measurements were more reliable than the density measurements. Figure 2(f) shows a statistical analysis of the SWNT diameters obtained from AFM measurements. The diameter distribution for most SWNTs was 0.7–1.8 nm, with an average diameter of 1.42 nm.

High-resolution transmission electron microscopy (HRTEM), which is a higher-resolution tool, can be used to directly observe SWNTs at the atomic scale [36, 37]. It can therefore be used for more accurate measurements of nanotube density. For SWNT arrays on a substrate surface, preparation of a HRTEM specimen is extremely difficult. The isolated SWNTs very easily form tube bundles or break during the transfer process [25, 38]. HRTEM images of horizontal SWNT arrays have rarely been reported, let alone ultra-high-density SWNT arrays, which are more challenging to obtain. In our previously reported work, the ultra-high-density SWNT arrays from Trojan catalysts were of small area and usually grew at the edge of the substrate; this further prevented transfer and use in other applications. Here, large-area, ultra-high-density SWNT arrays obtained using Trojan-Mo catalysts covered the full substrate. Through trial and error, we successfully transferred the ultra-high-density SWNT arrays grown on the sapphire surface to an ultra-thin carbon membrane supported on a Cu grid for HRTEM characterization (more details of the SWNT transfer process are given in the experimental section). Figures 2(g)–2(i) show typical TEM images at different magnifications. The SWNTs transferred onto the ultra-thin carbon membrane were well isolated and arranged in parallel, maintaining the original morphology on the sapphire. To distinguish the SWNTs from each other, high-magnification HRTEM, which would decrease the observation area, is needed. TEM observations at high magnification show that the local tube density can be as high as 160 tubes/μm (Fig. 2(i)). The slight increase in density compared with our previous results (as high as 130 SWNTs/μm) proved that the larger-area SWNT arrays synthesized using Trojan-Mo catalysts maintained their ultra-high density. Of course, it is still difficult to ensure the production of larger areas with well-distributed densities as high as 160 tubes/μm and sub-micron uniformity at this point. Nevertheless, this result is the highest reported density for grown SWNT arrays to date [26, 39]. A clear increase in the SWNT array area and preservation of the ultra-high density were achieved using this improved synthetic method, therefore it is important to investigate the detailed growth mechanism. Many reported studies of SWNT growth have shown that catalyst–substrate interactions strongly influence the catalytic efficiency, and these interactions are closely related to surface energies [35, 40]. Metal catalysts generally have higher surface energies than oxide substrates, leading to dewetting of metal catalysts on oxide substrates [40]. As a result, metal catalysts easily migrate and accumulate on the surfaces of oxide substrates. Fe, which has a higher surface energy than Mo, is expected to dewet more easily on sapphire surfaces [26].

This is supported by previous studies, which showed that metal species that are more electropositive are more likely to wet the oxide layer (e.g., Mo instead of Fe) [41]. Fe and Mo catalysts therefore show very different degrees of dewetting on sapphire, and Mo nanoparticles adhere better to *a*-plane sapphire than Fe nanoparticles do, which will restrain aggregation of active catalysts during SWNT growth [28, 29].

In order to confirm this speculation, $Fe(OH)_3$/ethanol solution and $(NH_4)_6Mo_7O_{24}\cdot 4H_2O/H_2O$ solution were dispersed on the surfaces of sapphire substrates by

spin coating. The precursors were reduced by H_2 at 830 ℃ for 5 min. Figures 3(a) and 3(b) show the AFM analysis of the sapphire surfaces; large agglomerated particles can be clearly observed for the Fe catalyst (Fig. 3(a)). The average diameter of the Fe nanoparticles was 7.36 nm (Fig. 3(e)). This phenomenon provides strong evidence that migration and aggregation of the Fe catalysts on sapphire were severe. In contrast, most of the Mo catalyst particles were smaller than 2 nm (Fig. 3(e)), and were suitable for SWNT growth. This observation indicates strong anchoring of the Mo nanoparticles on the sapphire surface. Figures 3(c) and 3(d) show AFM images of sapphire substrates loaded with Trojan-Mo catalysts after H_2 treatment at 830 ℃ for 5 and 30 min, respectively. We can see that with increased reduction time, the size distribution of the catalyst particles did not change much, and most of the catalyst particles were still smaller than 3 nm after H_2 reduction for 30 min (Fig. 3(e)). This is attributed to Mo nanoparticles stabilizing the released Fe Trojan catalysts [42, 43]. SWNT arrays with higher densities and larger growth areas were therefore obtained. In addition, the sapphire substrate loaded with Mo precursors after treatment at 830 ℃ in air for 30 min were characterized using X-ray photoelectron spectroscopy (XPS). The Mo 3d peaks (Fig. 3(f)) for the surface and bulk (3 nm depth) show that the Mo catalysts stayed on the surface, and did not dissolve into the sapphire substrate at the SWNT growth temperature.

On the basis of the above analysis, we propose that some of the Mo nanoparticles provided nucleation sites for the early stage of SWNT growth. With increasing time, the Mo catalyst particles and nanotubes grown from them suppressed the migration/agglomeration of the released Trojan catalyst. The synergistic effect of the Trojan-Mo catalysts resulted in expansion of the ultra-high-density SWNT array growth area. The process is schematically illustrated in Fig. 4(a). Control experiments were performed to verify our hypothesis. First, we compared the growth results under the same CVD conditions using different catalysts. When only Trojan catalysts were used for SWNT growth for 1 min, no SWNTs were found (Fig. 4(b)), and no

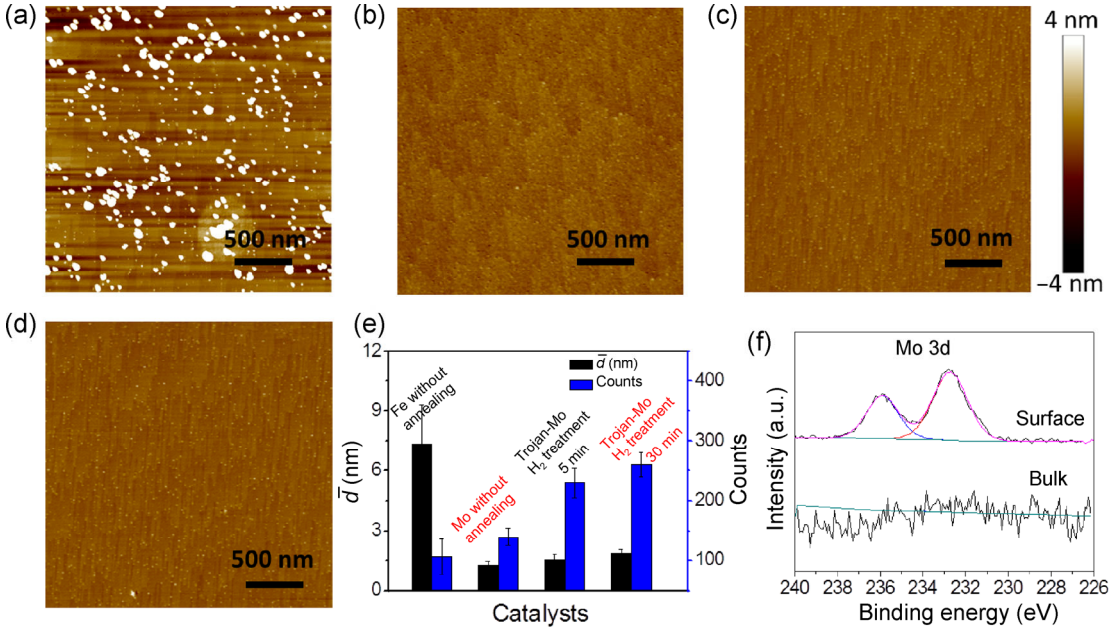

Figure 3 (a)–(c) AFM images of sapphire substrates loaded with different catalysts ((a): only Fe catalysts (without annealing), (b): only Mo catalysts (without annealing), (c): Trojan-Mo catalysts) after H_2 treatment at 830 °C for 5 min. (d) AFM images of sapphire substrates loaded with Trojan-Mo catalysts after H_2 treatment at 830 °C for 30 min. AFM images (a)–(d) are on the same *Z*-scale (−4 to 4 nm). (e) Statistics of corresponding counts and average diameters of catalyst particle in a given area (1 μm × 1 μm). The error bars for the counts and average diameters are standard deviations, calculated from five statistical results. (f) XPS spectra of Mo 3d peaks at surface and in bulk (3 nm depth) of sapphire substrate loaded with Mo precursors after heating for 30 min in air at 830 °C. Mo catalysts did not dissolve into the sapphire substrate at the SWNT growth temperature.

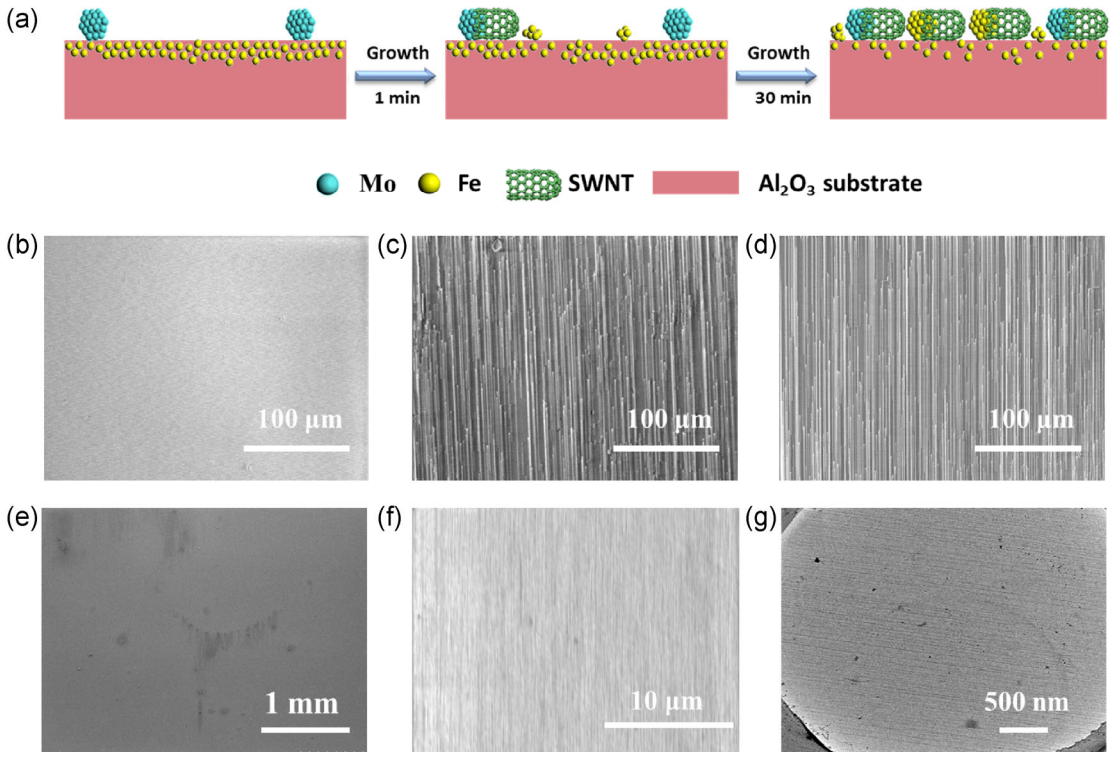

Figure 4 (a) Schematic illustration of Trojan-Mo catalysis of constant growth of SWNTs in CVD process. Mo nanoparticles that had nucleated for SWNT growth in advance of Fe gradually released and formed Fe nanoparticles. (b)–(d) SEM images of SWNTs grown from different catalysts ((b): only Trojan catalysts, (c): only Mo catalysts (without annealing), (d): Trojan-Mo catalysts) after SWNT growth for 1 min. SEM images (e) and (f) and HRTEM image (g) of ultra-high-density SWNT arrays over large areas using Trojan-Mo catalysts after SWNT growth for 30 min.

catalyst was found on the surface (Fig. S3(a) in the ESM). These results are in good agreement with our previous findings [26]. Trojan catalysts gradually released from the substrate need a certain time, and 1 min is not enough. However, Mo catalysts loaded on the sapphire surface did not undergo dissolution and release. They were able to nucleate and catalyze the growth of SWNTs in 1 min, as shown in Fig. 4(c). Large-area SWNT arrays of density ~1 tube/μm were obtained using Mo catalysts only. Similar results were observed using Trojan-Mo catalysts after growth for 1 min (Fig. 4(d)). The SWNT density increased with increasing growth time. Finally, horizontally aligned, large-area, uniform SWNT arrays (Figs. 4(e) and 4(f)) of ultra-high density (Fig. 4(g)) were obtained after growth for 30 min. In addition, the use of Mo catalysts only (without annealing at 1,100 °C) for SWNT growth for 30 min gave a final density of about 10 tubes/μm (Fig. S3(b) in the ESM). These results show that Mo catalysts stabilized the released Trojan catalysts and expanded the growth area, and made it possible to further increase the SWNT density by combining the advantages of Mo and Trojan catalysts.

The SWNT arrays synthesized using Trojan-Mo catalysts have much larger areas, while retaining attractively high densities, and are therefore more suitable for fabrication of large-current electronic devices [25, 44]. Figure 5(a) shows a schematic diagram of a SWNT field-effect transistor (FET) with a self-aligned U-gate structure [45]. The as-grown SWNTs on sapphire were directly fabricated into top-gate transistors. The gate stack consisted of YO_x/Ti and the source/drain electrodes were made of Ti (0.5 nm)/Pd (70 nm). Figure 5(b) shows SEM images of top-gated FETs made from these SWNT arrays, with a gate length L_g = 0.5 μm, channel length L_{ch} = 2 μm, and channel width W = 15 μm. The SWNT transistor is much wider than the SWNT array, therefore its on-current density is a much better indicator of the large-area tube density than TEM measurements. Figures 5(c) and 5(d) show

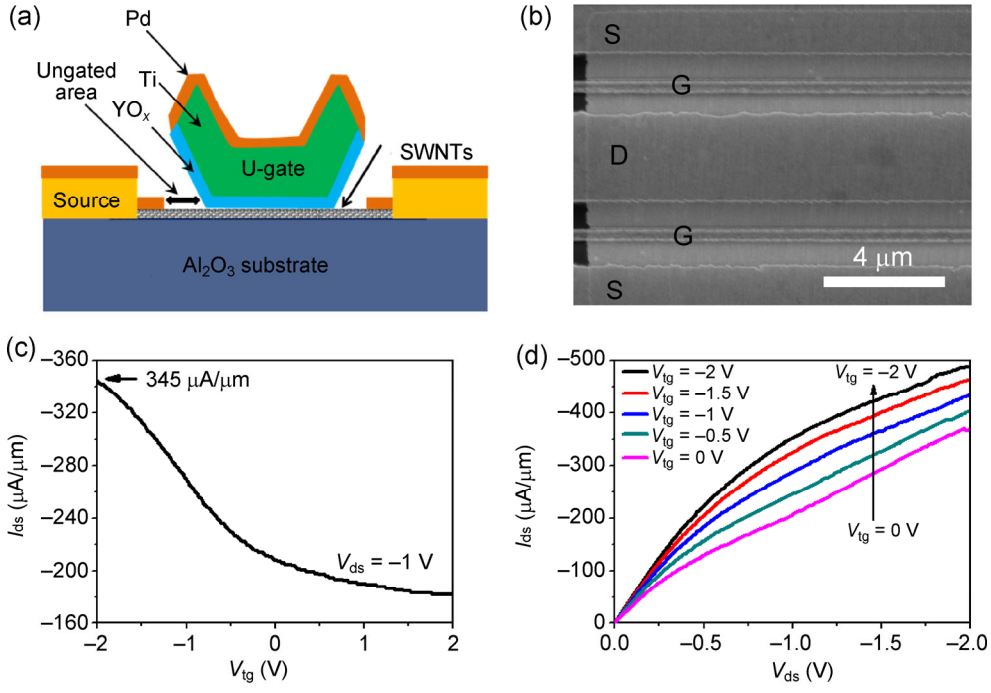

Figure 5 (a) Schematic illustration of ultra-high-density aligned SWNT FET with self-aligned U-gate structure. The horizontal dimension of each ungated area is about 100 nm. (b) SEM image showing core region of FET device fabricated on as-grown SWNT arrays with S, D, and G electrodes; W = 15 μm, L_{ch} = 2 μm, L_g = 0.5 μm. (c) Typical transfer characteristic curve of SWNT device with V_{ds} = −1 V. (d) Output characteristics of high-current-density devices. V_{tg} was varied from 0 to −2.0 V in steps of 0.5 V.

representative transfer and output characteristics of the fabricated FETs. The largest on-state current was −488 μA/μm at the drain-source voltage (V_{ds}) = the gate-source voltage (V_{gs}) = –2 V, which matched our previous best result of −467 μA/μm at V_{ds} = V_{gs} = –2 V, with a similar channel length. The corresponding on-conductance per width was 244 μS/μm, which is a useful parameter for comparison with the published data for the drive current [8, 9, 25, 26]. The remarkably high current density and on-conductance were strong evidence that the SWNT arrays grown using Trojan-Mo catalysts retained their ultra-high densities over large areas. These dense and perfectly aligned SWNTs with high current-carrying capabilities and large active areas are promising candidates for interconnectors in electronic applications.

3 Conclusions

In summary, we used a novel and effective catalyst design (Trojan-Mo catalysts) to successfully synthesize large-area, ultra-high-density (as high as 160 tubes/μm) SWNTs on sapphire surfaces. Detailed characterization verified that the Mo catalyst particles nucleated and suppressed agglomeration of Fe nanoparticles, resulting in expansion of the growth area of SWNT arrays, while retaining ultra-high density. In addition, transistors based on the as-grown SWNTs exhibited high current densities and on-conductances, showing the great potential of SWNTs in nanoelectronic applications. Trojan-Mo catalysts offer a range of choices for the structure-controlled growth of SWNT arrays. Further studies and optimization of the CVD conditions by our group are ongoing, to improve the SWNT electrical properties and chirality selection by careful use of Trojan-Mo catalysts. Finally, this work provides a better understanding of the mechanism of SWNT growth on surfaces and represents a step forward in large-area synthesis of ultra-high-density SWNT arrays on substrates.

4 Experimental

4.1 Synthesis of ultra-high-density, aligned SWNT arrays

Trojan catalysts were prepared as described in Ref. [26].

Briefly, $Fe(OH)_3$/ethanol solution (0.05 mmol/L) was dispersed on clean a-plane sapphire substrates (15 mm × 30 mm; Hefei Kejing Materials Technology Co.) and annealed at 1,100 ℃ in air for 8 h for dissolution into the substrate. Then $(NH_4)_6Mo_7O_{24}{\cdot}4H_2O/H_2O$ solution (0.05 mmol/L) was loaded onto the substrate by spin coating, without annealing at 1,100 ℃. The sapphire substrates containing Trojan-Mo catalysts were placed in a 1 inch tube and heated in air at 830 ℃. The system was purged with 300 standard cubic centimeters per minute (sccm) argon, and 100 sccm H_2 and 50 sccm argon were introduced through an ethanol bubbler for the growth of ultra-high-density SWNT arrays. After growth for 30 min, the H_2 was turned off and the furnace was cooled to room temperature in an argon atmosphere.

4.2 Transfer of ultra-high-density, aligned SWNT arrays onto ultra-thin carbon membrane

A poly(methyl methacrylate) (PMMA) solution (M_W = 950,000, 4 wt.%) was spin coated onto the sapphire substrate and baked at 170 ℃ for 10 min to form a thin film that encapsulated the SWNT arrays. This PMMA/SWNTs film was separated from the sapphire substrate in KOH aqueous solution (1 mol/L, 70 ℃). Before the PMMA/SWNTs film was attached to the ultra-thin carbon membrane supported on a Cu grid, an ethanol solution was dropped onto the ultra-thin carbon membrane to wet it. Next, the membrane was dried at 50 ℃ for 1 h. This provides tight contact between the ultra-thin carbon membrane and the PMMA/SWNTs film. Finally, the PMMA film was removed by decomposition at 320 ℃ in an argon atmosphere for 2.5 h.

4.3 Characterization

The structures of the as-grown SWNTs and catalysts were studied using SEM (S4800 field-emission instrument, Hitachi, Japan), HRTEM (Tecnai F30, FEI), AFM (Veeco NanoScope IIIA, Veeco Co.), Raman spectroscopy (Horiba HR800 Raman system), and XPS (ESCALab250, Thermo Scientific Corporation).

4.4 Fabrication of FET device and performance measurements

Top-gated FETs based on the as-grown SWNT arrays were fabricated through a self-aligned U-gate process [45]. Electron-beam lithography was used to define the gate and contact electrodes. The gate length was 0.5 μm, the source and drain electrodes were deposited by electron-beam evaporation of Ti/Pd (0.5/70 nm), and then Pd (10 nm) was deposited as a self-aligned contact electrode. The direct-current characteristics of our devices were determined in air using a semiconductor analyzer (Keithley 4200 SCS).

Acknowledgements

This work was supported by the National Natural Science Foundation of China (Nos. 21233001, 21129001, 51272006, 51432002, and 51121091), the National Basic Research Program of China (No. 2011CB932601) and Beijing Municipal Science and Technology Commission (No. D141100000614001).

Electronic Supplementary Material: Supplementary material (further details of SEM images of SWNT arrays and AFM images of the sapphire substrate) is available in the online version of this article at http://dx.doi.org/10.1007/s12274-015-0869-9.

References

[1] Avouris, P.; Chen, Z. H.; Perebeinos, V. Carbon-based electronics. *Nat. Nanotechnol.* **2007**, *2*, 605–615.

[2] Che, Y. C.; Chen, H. T.; Gui, H.; Liu, J.; Liu, B. L.; Zhou, C. W. Review of carbon nanotube nanoelectronics and macroelectronics. *Semicond.Sci. Technol.* **2014**, *29*, 073001.

[3] Kang, L. X.; Hu, Y.; Liu, L. L.; Wu, J. X.; Zhang, S. C.; Zhao, Q. C.; Ding, F.; Li, Q. W.; Zhang, J. Growth of close-packed semiconducting single-walled carbon nanotube arrays using oxygen-deficient TiO_2 nanoparticles as catalysts. *Nano Lett.* **2015**, *15*, 403–409.

[4] Tulevski, G. S.; Franklin, A. D.; Frank, D.; Lobez, J. M.; Cao, Q.; Park, H.; Afzali, A.; Han, S.-J.; Hannon, J. B.; Haensch, W. Toward high-performance digital logic technology with carbon nanotubes. *ACS Nano* **2014**, *8*, 8730–8745.

[5] Franklin, A. D. Electronics: The road to carbon nanotube transistors. *Nature* **2013**, *498*, 443–444.

[6] Wang, C.; Ryu, K.; Arco, L.; Badmaev, A.; Zhang, J. L.; Lin, X.; Che, Y. C.; Zhou, C. W. Synthesis and device applications of high-density aligned carbon nanotubes using low-pressure chemical vapor deposition and stacked multiple

transfer. *Nano Res.* **2010**, *3*, 831–842.

[7] Shulaker, M. M.; Wei, H.; Patil, N.; Provine, J.; Chen, H.-Y.; Wong, H. S. P.; Mitra, S. Linear increases in carbon nanotube density through multiple transfer technique. *Nano Lett.* **2011**, *11*, 1881–1886.

[8] Cao, Q.; Han, S.-J.; Tulevski, G. S.; Zhu, Y.; Lu, D. D.; Haensch, W. Arrays of single-walled carbon nanotubes with full surface coverage for high-performance electronics. *Nat. Nanotechnol.* **2013**, *8*, 180–186.

[9] Brady, G. J.; Joo, Y.; Wu, M.-Y.; Shea, M. J.; Gopalan, P.; Arnold, M. S. Polyfluorene-sorted, carbon nanotube array field-effect transistors with increased current density and high on/off ratio. *ACS Nano* **2014**, *8*, 11614–11621.

[10] Cao, Q.; Han, S.-J.; Tulevski, G. S. Fringing-field dielectrophoretic assembly of ultrahigh-density semiconducting nanotube arrays with a self-limited pitch. *Nat. Commun.* **2014**, *5*, 5071.

[11] Park, S.; Pitner, G.; Giri, G.; Koo, J. H.; Park, J.; Kim, K.; Wang, H. L.; Sinclair, R.; Wong, H. S. P.; Bao, Z. Large-area assembly of densely aligned single-walled carbon nanotubes using solution shearing and their application to field-effect transistors. *Adv. Mater.* **2015**, *27*, 2656–2662.

[12] Wang, Y. L.; Pillai, S. K. R.; Chan-Park, M. B. High-performance partially aligned semiconductive single-walled carbon nanotube transistors achieved with a parallel technique. *Small* **2013**, *9*, 2960–2969.

[13] Chen, Y. B.; Zhang, J. Chemical vapor deposition growth of single-walled carbon nanotubes with controlled structures for nanodevice applications. *Acc. Chem. Res.* **2014**, *47*, 2273–2281.

[14] Feng, C. Q.; Yao, Y. G.; Zhang, J.; Liu, Z. F.Nanobarrier-terminated growth of single-walled carbon nanotubes on quartz surfaces. *Nano Res.* **2009**, *2*, 768–773.

[15] Chen, Y. B.; Zhang, Y. Y.; Hu, Y.; Kang, L. X.; Zhang, S. C.; Xie, H. H.; Liu, D.; Zhao, Q. C.; Li, Q. W.; Zhang, J. State of the art of single-walled carbon nanotube synthesis on surfaces. *Adv. Mater.* **2014**, *26*, 5898–5922.

[16] Zhou, W. W.; Rutherglen, C.; Burke, P. J. Wafer scale synthesis of dense aligned arrays of single-walled carbon nanotubes. *Nano Res.* **2008**, *1*, 158–165.

[17] Zhang, Y. Y.; Zhang, Y.; Xian, X. J.; Zhang, J.; Liu, Z. F. Sorting out semiconducting single-walled carbon nanotube arrays by preferential destruction of metallic tubes using xenon-lamp irradiation. *J. Phys. Chem. C* **2008**, *112*, 3849–3856.

[18] Ding, L.; Zhou, W. W.; McNicholas, T. P.; Wang, J. Y.; Chu, H. B.; Li, Y.; Liu, J. Direct observation of the strong interaction between carbon nanotubes and quartz substrate. *Nano Res.* **2009**, *2*, 903–910.

[19] Li, Y.; Cui, R. L.; Ding, L.; Liu, Y.; Zhou, W. W.; Zhang, Y.; Jin, Z.; Peng, F.; Liu, J. How catalysts affect the growth of single-walled carbon nanotubes on substrates. *Adv. Mater.* **2010**, *22*, 1508–1515.

[20] Zhou, W. W.; Ding, L.; Liu, J. Role of catalysts in the surface synthesis of single-walled carbon nanotubes. *Nano Res.* **2009**, *2*, 593–598.

[21] He, M. S.; Duan, X. J.; Wang, X.; Zhang, J.; Liu, Z. F.; Robinson, C. Iron catalysts reactivation for efficient CVD growth of SWNT with base-growth mode on surface. *J. Phys. Chem. B* **2004**, *108*, 12665–12668.

[22] Chen, Y. B.; Zhang, J. Diameter controlled growth of single-walled carbon nanotubes from SiO_2 nanoparticles. *Carbon* **2011**, *49*, 3316–3324.

[23] Hong, S. W.; Banks, T.; Rogers, J. A. Improved density in aligned arrays of single-walled carbon nanotubes by sequential chemical vapor deposition on quartz. *Adv. Mater.* **2010**, *22*, 1826–1830.

[24] Wu, B.; Geng, D. C.; Guo, Y. L.; Huang, L. P.; Chen, J. Y.; Xue, Y. Z.; Yu, G.; Liu, Y. Q.; Kajiura, H.; Li, Y. M. Ultrahigh density modulation of aligned single-walled carbon nanotube arrays. *Nano Res.* **2011**, *4*, 931–937.

[25] Zhou, W. W.; Ding, L.; Yang, S.; Liu, J. Synthesis of high-density, large-diameter, and aligned single-walled carbon nanotubes by multiple-cycle growth methods. *ACS Nano* **2011**, *5*, 3849–3857.

[26] Hu, Y.; Kang, L. X.; Zhao, Q. C.; Zhong, H.; Zhang, S. C.; Yang, L. W.; Wang, Z. Q.; Lin, J. J.; Li, Q. W.; Zhang, Z. Y. et al. Growth of high-density horizontally aligned SWNT arrays using Trojan catalysts. *Nat. Commun.* **2015**, *6*, 6099.

[27] Hong, G.; Chen, Y. B.; Li, P.; Zhang, J. Controlling the growth of single-walled carbon nanotubes on surfaces using metal and non-metal catalysts. *Carbon* **2012**, *50*, 2067–2082.

[28] Ago, H.; Uehara, N.; Ikeda, K.-I.; Ohdo, R.; Nakamura, K.; Tsuji, M. Synthesis of horizontally-aligned single-walled carbon nanotubes with controllable density on sapphire surface and polarized Raman spectroscopy. *Chem. Phys. Lett.* **2006**, *421*, 399–403.

[29] An, L.; Owens, J. M.; McNeil, L. E.; Liu, J. Synthesis of nearly uniform single-walled carbon nanotubes using identical metal-containing molecular nanoclusters as catalysts. *J. Am. Chem. Soc.* **2002**, *124*, 13688–13689.

[30] Dresselhaus, M. S.; Dresselhaus, G.; Saito, R.; Jorio, A. Raman spectroscopy of carbon nanotubes. *Phys. Rep.* **2005**, *409*, 47–99.

[31] Youn, S. K.; Park, H. G. Morphological evolution of Fe–Mo bimetallic catalysts for diameter and density modulation of vertically aligned carbon nanotubes. *J. Phys. Chem. C* **2013**, *117*, 18657–18665.

[32] Li, J.; He, Y. J.; Han, Y. M.; Liu, K.; Wang, J. P.; Li, Q. Q.; Fan, S. S.; Jiang, K. L. Direct identification of metallic and semiconducting single-walled carbon nanotubes in scanning electron microscopy. *Nano Lett.* **2012**, *12*, 4095–4101.

[33] Kocabas, C.; Kang, S. J.; Ozel, T.; Shim, M.; Rogers, J. A. Improved synthesis of aligned arrays of single-walled carbon nanotubes and their implementation in thin film type transistors. *J. Phys. Chem. C* **2007**, *111*, 17879–17886.

[34] Homma, Y.; Suzuki, S.; Kobayashi, Y.; Nagase, M.; Takagi, D. Mechanism of bright selective imaging of single-walled carbon nanotubes on insulators by scanning electron microscopy. *Appl. Phys. Lett.* **2004**, *84*, 1750–1752.

[35] Petit, P.; Salem, D.; He, M. S.; Paillet, M.; Parret, R.; Sauvajol, J.-L.; Zahab, A. Study of the thermal stability of supported catalytic nanoparticles for the growth of single-walled carbon nanotubes with narrow diameter distribution by chemical vapor deposition of methane. *J. Phys. Chem. C* **2012**, *116*, 24123–24129.

[36] Lin, M.; Ying Tan, J. P.; Boothroyd, C.; Loh, K. P.; Tok, E. S.; Foo, Y.-L. Direct observation of single-walled carbon nanotube growth at the atomistic scale. *Nano Lett.* **2006**, *6*, 449–452.

[37] Yang, F.; Wang, X.; Zhang, D. Q.; Yang, J.; Luo, D.; Xu, Z. W.; Wei, J. K.; Wang, J.-Q.; Xu, Z.; Peng, F. et al. Chirality-specific growth of single-walled carbon nanotubes on solid alloy catalysts. *Nature* **2014**, *510*, 522–524.

[38] He, Y. J.; Li, D. Q.; Li, T. Y.; Lin, X. Y.; Zhang, J.; Wei, Y.; Liu, P.; Zhang, L. N.; Wang, J. P.; Li, Q. Q. et al. Metal-film-assisted ultra-clean transfer of single-walled carbon nanotubes. *Nano Res.* **2014**, *7*, 981–989.

[39] Ding, L.; Yuan, D. N.; Liu, J. Growth of high-density parallel arrays of long single-walled carbon nanotubes on quartz substrates. *J. Am. Chem. Soc.* **2008**, *130*, 5428–5429.

[40] Fu, Q.; Wagner, T. Interaction of nanostructured metal overlayers with oxide surfaces. *Surf.Sci. Rep.* **2007**, *62*, 431–498.

[41] Campbell, C. T. Ultrathin metal films and particles on oxide surfaces: Structural, electronic and chemisorptive properties. *Surf.Sci. Rep.* **1997**, *27*, 1–111.

[42] Zhao, M.-Q.; Zhang, Q.; Zhang, W.; Huang, J.-Q.; Zhang, Y. H.; Su, D. S.; Wei, F. Embedded high density metal nanoparticles with extraordinary thermal stability derived from guest-host mediated layered double hydroxides. *J. Am. Chem. Soc.* **2010**, *132*, 14739–14741.

[43] Amama, P. B.; Pint, C. L.; Kim, S. M.; McJilton, L.; Eyink, K. G.; Stach, E. A.; Hauge, R. H.; Maruyama, B. Influence of alumina type on the evolution and activity of alumina-supported Fe catalysts in single-walled carbon nanotube carpet growth. *ACS Nano* **2010**, *4*, 895–904.

[44] Peng, L.-M.; Zhang, Z. Y.; Wang, S. Carbon nanotube electronics: Recent advances. *Mater.Today* **2014**, *17*, 433–442.

[45] Ding, L.; Wang, Z. X.; Pei, T.; Zhang, Z. Y.; Wang, S.; Xu, H. L.; Peng, F.; Li, Y.; Peng, L.-M. Self-aligned U-gate carbon nanotube field-effect transistor with extremely small parasitic capacitance and drain-induced barrier lowering. *ACS Nano* **2011**, *5*, 2512–2519.